Preprints.org

Article

Not peer-reviewed version

Hydrogen vs. Energy Storage in Offshore Deep Depths Salt Caverns Drilled at Vadu, Constanta County, Romania

Sorinel Popescu , Stela Dinescu , Sorin Mihai Radu , Bogdan Tudor Obreja , Iulian Vlăducă * ,
Theodor Mihnea Sîrbu , Ramona Manuela Stanciuc , Mirela-Letitia Vasile

Posted Date: 17 February 2025

doi: 10.20944/preprints202502.1207.v1

Keywords: deep salt caverns; high pressure hydrogen storage; Romanian Energy Strategy

doi:10.20944/preprints202502.1207.v1

Article

Hydrogen vs. Energy Storage in Offshore Deep Depths Salt Caverns Drilled at Vadu, Constanta County, Romania

Sorinel Popescu [1], Stela Dinescu [2], Sorin Mihai Radu [3], Bogdan Tudor Obreja [4], Iulian Vlăducă [5,*], Mihnea Theodor Sîrbu [6], Ramona Manuela Stanciuc [7] and Mirela Letiţia Vasile [8]

1 University of Petrosani, Department of Mechanical, Industrial and Transport Engineering, 20 University Street, Petrosani, Romania
2 University of Petrosani, Department of Mechanical, Industrial and Transport Engineering, 20 University Street, Petrosani, Romania
3 University of Petrosani, Department of Mechanical, Industrial and Transport Engineering, 20 University Street, Petrosani, Romania
4 Horia Hulubei National Institute, No. 30, Reactorului Street, Magurele, Ilfov, Romania
5 National Research and Development Institute for Gas Turbines COMOTI, 220D Ave. Iuliu Maniu, 061126, Bucharest, Romania
6 National Research and Development Institute for Gas Turbines COMOTI, 220D Ave. Iuliu Maniu, 061126, Bucharest, Romania
7 National Research and Development Institute for Gas Turbines COMOTI, 220D Ave. Iuliu Maniu, 061126, Bucharest, Romania
8 National Research and Development Institute for Gas Turbines COMOTI, 220D Ave. Iuliu Maniu, 061126, Bucharest, Romania
* Correspondence: iulian.vladuca@comoti.ro; Tel.: 0040729058551

Abstract: The deep underground salt cavities have the advantage of allowing storage of hydrogen at higher pressures than surface installations. Worldwide, in the 2020s there were 4 functional sites of salt caverns used as hydrogen deposits, three in the United States and one in the United Kingdom, at an average of 600,000 m^3 capacity each at pressures varies between 50 - 150 bar in the United States and 3 x 70,000 m^3 at a pressure of 45 bar in the United Kingdom [1, 2]. From 2020 until now, there is an increase in the salt deposit development for hydrogen storage, expecting to account for about 18% of global energy demand by 2050 [3]. Near Vadu locality, Constanta County, Romania, there are sald deposits located between 705 m and 905 m, respectively 1542 m and 1778 m, offshore in the Black Sea continental shelf. The study consists in determining the storage capacity, at the two drilling depths, for reliable projects of hydrogen storage, for Romania's Energy Strategy, leading to a reduction in the carbon footprint at 70% in 2050 compared to the levels recorded in 2008 of CO_2 emissions per transport unit for all the civilian or military transport ships [4, 5].

Keywords: deep salt caverns; high pressure hydrogen storage; Romanian Energy Strategy

---

1. Introduction

The continental shelf of the Black Sea represents the seabed, and the subsoil of the adjacent submarine regions located beyond the territorial sea to a depth of 200 m or over this limit, up to the point where the depth of the waters allows the exploitation of the natural resources of these regions. The platform has the appearance of a plane with a very low slope that descends towards the sea, reaching depths of 200 m [6], see also Figure 1, (a). The intermediate depths (50-100 m) follow the shoreline and include the territorial sea (22 km from onshore) and the exclusive economic zone, further on it being the free zone. The map from Figure 1, (b) shows a research work of a romanian-bulgarian team for determining simultaneously the bathymetry, gravimetry and total field magnetometry, with the R/V Mare Nigrum GeoEcoMar's ship (Romania) [7, 8], that covered a total shelf and slope area of 47,000 km², see in Figure 2, (b), the marked area [9]. The degree of knowledge

Preprints.org (www.preprints.org) | NOT PEER-REVIEWED | Posted: 17 February 2025 doi:10.20944/preprints202502.1207.v1

of the geology of the aquatic area, near the shore, encourages the elaboration of works that capitalize the information already obtained; the geological exploration of the Romanian continental platform of the Black Sea has a long history, marking almost 55 years since the recording of the first seismic sections and 45 years since the digging of the first well. From a seismological, gravity and magnetic point of view it is evaluated an area of approx. 33,160 km², and in the same time 120 wells were dug, that share the research in three subunits, North Dobrogea, Central Dobrogea and Southern Dobrogea, see Figure 1, (c, d) whose differences are manifested especially at the foundation level, 57 of them being between two geological faults, Capidava-Ovidiu and Peceneaga-Camena, that mark the Central Dobrogea area [9].

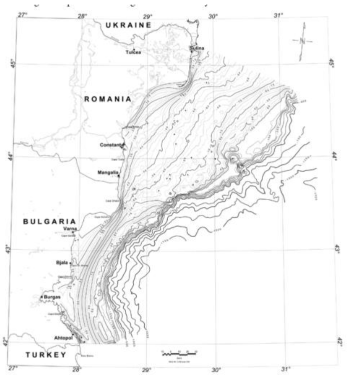

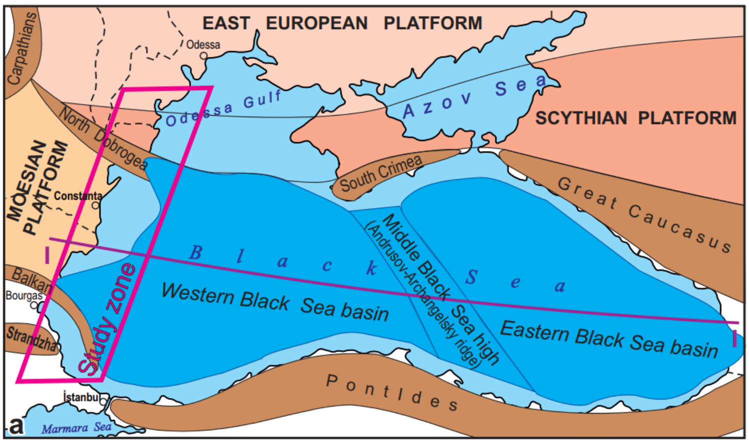

(a) (b)

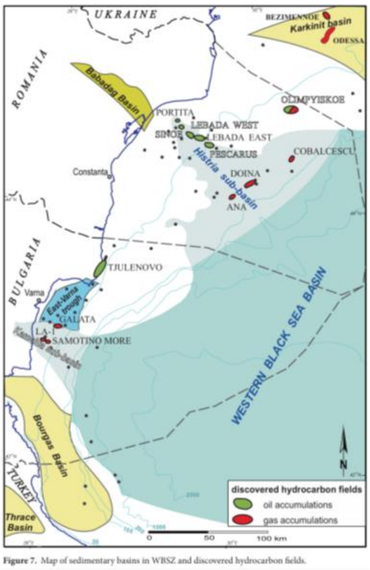

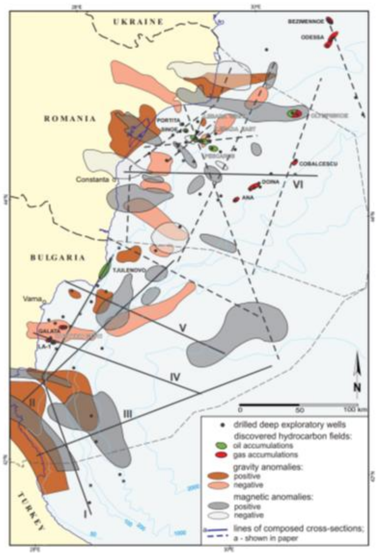

(c) (d)

Figure 1. The continental shelf of the Western Black Sea Basin; (**a**) Bathimetry map; (**b**) Romanian-bulgarian team research work area with the main faults depicted; (**c**) The wells that were dug, that share the research in three subunits, North Dobrogea, Central Dobrogea and Southern Dobrogea; (**d**) Evaluated an area of approx. 33,160 km² from a seismological, gravity and magnetic point of view.

In Figure 2, a detail of Figure 1, (d) was made where it has been suggested that in the Vadu area there is a gravity negative anomaly which can be interpreted by various authors as salt deposits.

Preprints.org (www.preprints.org) | NOT PEER-REVIEWED | Posted: 17 February 2025 doi:10.20944/preprints202502.1207.v1

Gravimetry is usually used for salt deposits, and it is not used for deposits that contain iron [10, 11, 12].

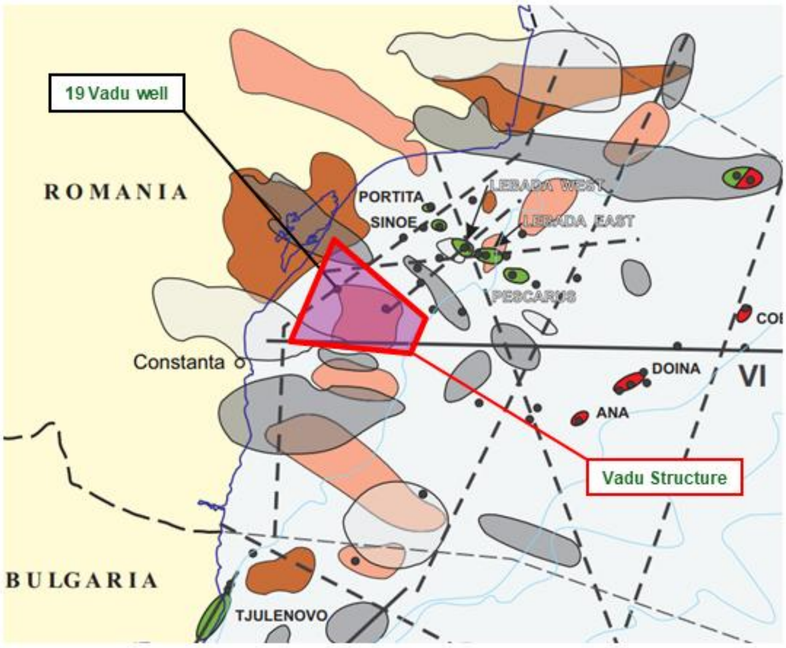

Figure 2. The exploratory wells and gravity anomalies in the Moesic Platform - Central Dobrogea. Details of Figure 1, (d).

As a whole, the geological structure of the Dobrogean continental platform includes the same major units as the adjacent land: the North-Dobrogean Orogen, the Babadag Basin and the Moesic Platform with its subdivisions, Central Dobrogea and Southern Dobrogea, see also Figure 3 [13].

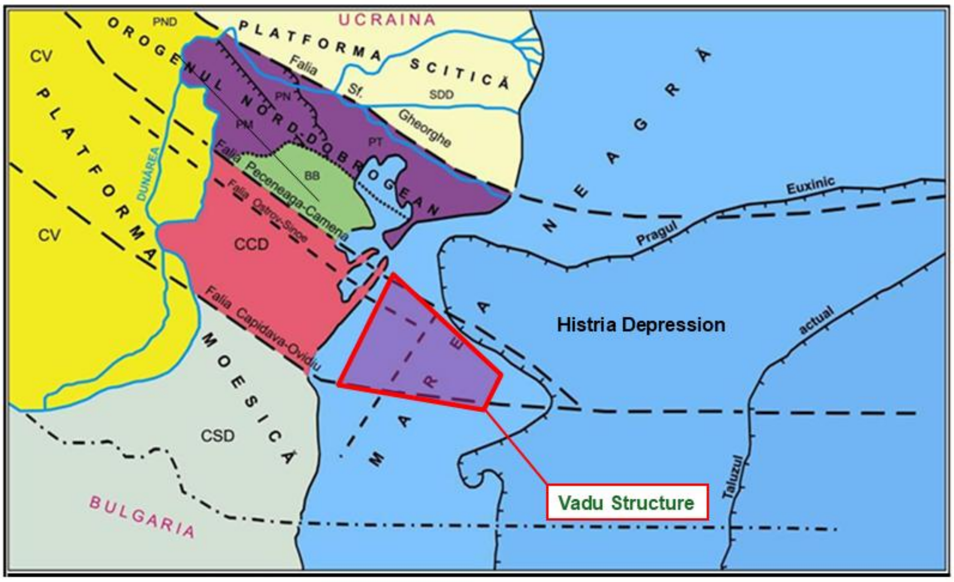

Figure 3. The major structural units that make up the southeastern part of Romania's territory and subunits of the North-Dobrogean Orogen, Babadag Basin, Central Dobogea and South Dobrogea.

The paper is studying the Vadu structure that is before the Histria Depression, and is situated in Central Dobrogea, see the Figures 2, and 3. The Vadu structure represented by the evaporitic facies from the Upper Jurassic and Lower Cretaceous periods, a unique case in the Romanian sector of the Black Sea continental platform, is mainly composed of salt alternating with limestone. These facies were opened by the 19 Vadu well, at a depth of about 1,500 m, in the interval 620 m ÷ 2,110 m.

Preprints.org (www.preprints.org) | NOT PEER-REVIEWED | Posted: 17 February 2025 doi:10.20944/preprints202502.1207.v1

Towards the east of the basin, these facies are replaced by carbonates [14]. The Callovian-Oxfordian, 2,036 m ÷ 2,110 m is predominantly sandstone with clay intercalations, the Oxfordian – Kimmeridgian, 2,036 m ÷1,965 m is predominantly calcareous with marl intercalations, the Kimmeridgian – Purbekian, 1,818 m ÷ 1,965 m is represented by alternations of argillaceous limestone and limestone dolomitic. The Purbekian-Wealdian follows, 1,820 m ÷ 620 m represented by rock salt, alternating with calcareous - dolomitic or bituminous shale and anhydrite. The evaporitic series passes into the Neocomian, 620 m ÷ 458 m to gypsums with anhydrite. In succession, the Neocominan passes to limestone and conglomerates. In Apţian, 389 m ÷ 458 m the series continues also with conglomerates/pebbles and limestone. The Upper Cretaceous, 311 m ÷ 389 m, is calcareous and sandstone-clay with marl intercalations. The Upper Paleogene, 389 m ÷ 250 m is transgressive, being made up of sandstones and marly sandstones or with clayey intercalations. The Vadu structure was investigated in 1988 – 1989, when the 19 Vadu borehole was dug see Figure 4 [15]. The saline formation that is the object of this study was attributed to the Purbekian-Wealdian. The character of the deposits and the great thickness of the saline formation seem to represent the indicators of a sabkha-type sedimentary environment developed on a platform with very active subsidence [15].

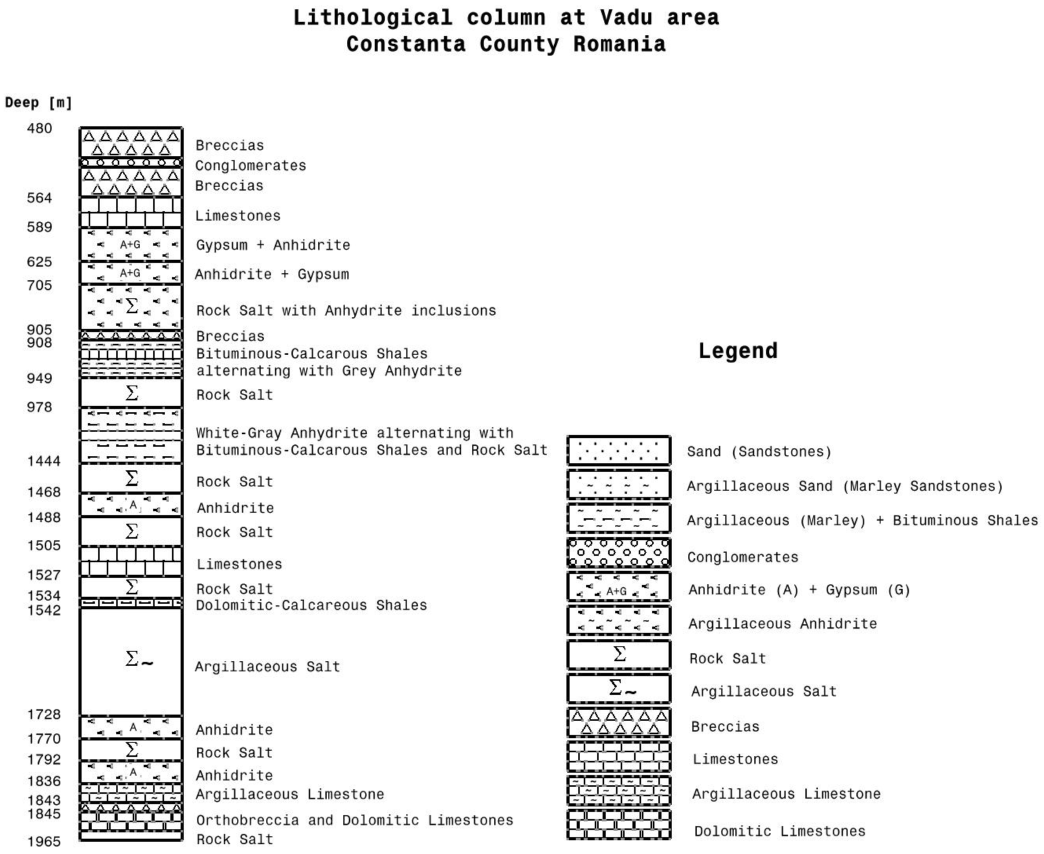

Figure 4. The lithostratigraphic column of well 19 Vadu, Constanta County Romania.

2. The Evaluation Methodology for the Deep Salt Deposit in the Continental Shelf of the Black Sea and Calculus Results for Energy Storage Potential

The section methodology and evaluation of caverns for hydrogen storage summarizes the offshore salt cavern site selection process starting with the characterization of salt deposits, then passing the choice of conditions considered suitable for cavern development by analyzing the proximity of existing infrastructure and finally, on cavern design, placement and storage capacity estimates.

Determining the development potential of salt caverns requires the use of multiple techniques and datasets to form a robust analysis of the geology and geophysics of salt formations and associated

Preprints.org (www.preprints.org) | NOT PEER-REVIEWED | Posted: 17 February 2025 doi:10.20944/preprints202502.1207.v1

geomechanics to ensure cavern stability and subsequent energy security. Therefore, characterizing the identified salt formations and evaluating them for their suitability for hydrogen storage are the first steps in the screening process. The selection process for the depth and height of the location of the caverns was based on the lithological heterogeneity, thickness and mode of formation: sedimentary or diapiric. The cavern placement was based on an optimal depth range dependent on the convergence rate of the caverns, hydrogen storage pressure, floor and safety pillar thickness, and recommended cavern shape criteria established from the literature and gas storage experience underground see Figure 5 (**a**) [16], Figure 5 (**b**) [16] and Table 1 [17].

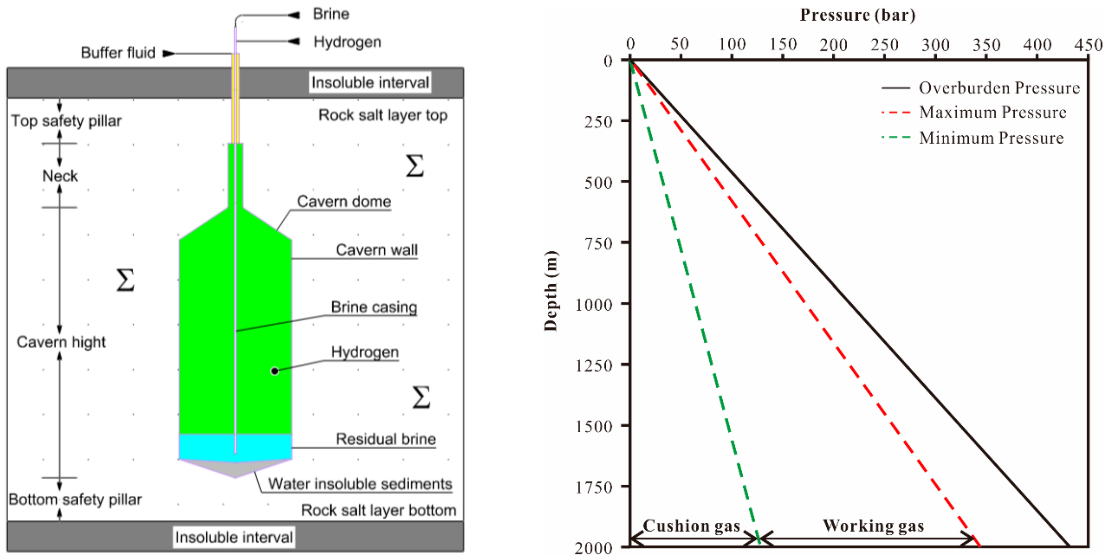

(**a**) (**b**)

Figure 5. Simplified schematic diagram for a cavern design: (a) Usual capsule shape, for geotechnical safety, and (b) Safety depth for the cavern vs. Geostatic + Hydrostatic pressure.

Table 1. Key parameters in cavern design.

Parameters	Values	References
Distance between caverns (axis to axis)	4 times the cavern diameter	Caglayan et al. (2020) [18]
Ceiling-wall thickness	75% from cavern diameter	Caglayan et al. (2020) [18]
Foot-wall thickness	20% from cavern diameter	L. Wang et al. (2015) [19]
Height / Diameter ratio	> 0,5	T. Wang et al. (2015) [20]
The shape of the caverns	Bell-shaped or cylindrical	Lux (2009) [21]
The depth range where from the cavern begin to be formed	500 - 3000m	Evans and Holloway (2009) [22] Plaat (2009) [23] Caglayan et al. (2020) [18]
Distance from adjacent faults/ discontinuities or old workings (e.g. abandoned oil wells)	> 2 times the cavern diameter	L. Wang et al. (2015) [19]

Preprints.org (www.preprints.org) | NOT PEER-REVIEWED | Posted: 17 February 2025 doi:10.20944/preprints202502.1207.v1

H_2 operating pressure (measured at the bottom of the cemented column)	P_{min}=24%, P_{max}=80% from geostatic pressure	Ozarslan (2012); [24] Stolzenburg et al. (2014) [25]
Distance from salt formation edge (dome margins)	> 500m (diapiric) > 2000m (sedimentary)	Kupfer et al. (1998) [26] Caglayan et al. (2020) [18]

The classical method consists in injecting fresh water into the saline layer; the fresh water circulates and becomes salty, forming the brine, which is then extracted through extraction pipes and directed for processing and production, especially of sodium products. The equipment consists of three concentric columns: a sealing column (anchoring column, cemented, which will have the length to where it is estimated that the ceiling of the future dissolution gap should be), an exploitation column (cassing) and a column extraction (tubing). Three concentric spaces are created, which ensure that the circuits of the cell are three technological fluids: industrial water, insulating fluid and brine [27]. In our case at Vadu well, the induistrial water can be marine water, and, also, the brine can be discharged back into the sea, as no facilities for salt processing are implemented yet. The construction of the well begins with the drilling of the well for the anchor column, continues with its tubing, cementing, tightness check and finishing with the drilling and tubing of the exploitation hole see Figure 6 (a) [28]. In Figure 6 (b) the cavern was simplified to a cylinder with conical top and bottom with the values of: Ød~300mm – the diameter of the cemented column, ØD – the diameter of the underground cavern, h_1 = 1/3D, h_3 = 1/6D, h_2 = H-(h_1 + h_3), where H is the total hight of the cavern.

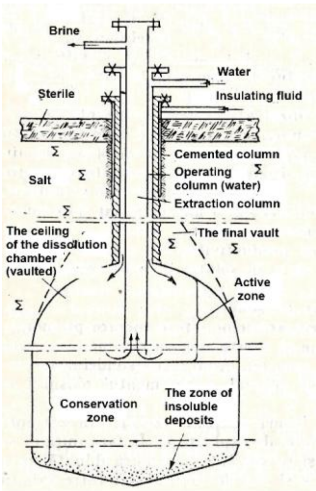

(**a**)

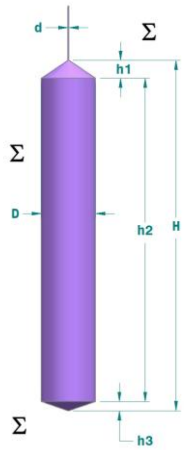

(**b**)

Figure 6. Simplified schematic diagram for a cavern design; (**a**) Theoretical extraction of brine; (**b**) Simplified cavern, where:.

The volume of the simplified cavern from Figure 7 (b) is given by the relation:

$$V = \frac{\pi}{12} \cdot D^2 \cdot (3 \cdot H - D) \text{ [m]} \quad (1)$$

The conditions for carrying out marine drilling are more special, considering the lack of fresh water. However, the Black Sea has a medium to low salinity around the Vadu structure. For the area near the coast, the values for temperature and salinity measured in June are in the range of 20.68°C - 26.2°C, respectively 9.8 PSU (practical salinity unit – 9.8 g salt/1000g water) in the Danube mouth area and 17.98 PSU in the Vadu - Constanta - Eforie areas, see Figure 7 [29].

Preprints.org (www.preprints.org) | NOT PEER-REVIEWED | Posted: 17 February 2025 doi:10.20944/preprints202502.1207.v1

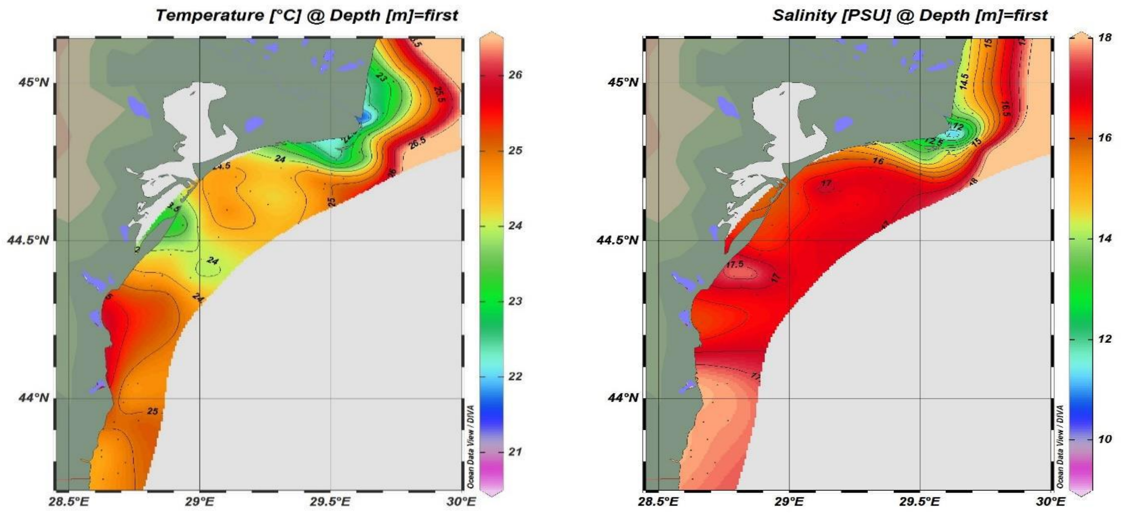

(**a**) (**b**)

Figure 7. Horizontal surface distribution of temperature and salinity in the coastal / exclusive economic zone during June 2022; (**a**) Temperature [°C] @ Depth [m]; (**b**) Salinity [PSU] @ Depth [m].

Another condition, according to the Romanian experience in the exploitation of salt through wells, is imposed by the depth: it is estimated that up to 1250 m there are no special technical problems [15]. On the world level, with the taking of additional measures, salt was also exploited from depths up to 3000 m. For example, since 1972, the company KemOne has been extracting the salt from deep caverns (1500–3000 m) in the form of brine [30]. In the Vadu structure, the exploitation of salt in order to create natural gas storage deposits is leased on the intervals of 705 - 905 m and 1542 - 1800 m. In the laboratories of the University of Petroşani, Petroşani city Romania, research was carried out on the samples of salt extracted from the 19 Vadu well to determine the geomechanical characteristics of rock salt, namely: physical-mechanical, deformation and rheological. The average values of these characteristics are shown in Table 2 [15]. In Table 3 [15], compressive strength measurements performed on salt samples from different salt mines in Romania are presented comparatively.

Table 2. The geomechanical properties of the salt from the 19 Vadu well.

Physically				Mechanically					Elastically		
Specific distance $\gamma \cdot 10^4$[N/m^3]	Apparent specific gravity $a \cdot 10^4$[N/m^3]	Porosity n[%]	Humidity W[%]	Compressive strength σ_{rc},[MPa]	Tensile strength σ_{rt}, [MPa]	Flexural strength σ_{rf}, [MPa]	Cohesion C [MPa]	The angle of internal friction φ, [^{0}]	The modulus of elasticity E [MPa]	The tension at the dilatation threshold σ_d [MPa]	Wave propagation speed v[m/s]

2.175 - 2.181	2.04 - 2.059	0.82 - 1.231	2.13 - 3.13	21.94 - 36.76	0.80 - 2.154	9.75 - 13.00	1.20 - 4.42	39 - 42	2120 - 2610	12.94 - 15.65	3885 - 4215

Table 3. Average compression strength of salt comparative table from different salt mines in Romania.

Deposit	Praid	Ocna Dej	Ocnele Mari	Tg. Ocna	Slanic Prahova	Vadu
Romanian County	Harghita	Cluj	Valcea	Bacau	Prahova	Constanta
Compression strength	21.7 [MPa]	21.1 [MPa]	18.3 [MPa]	25 [MPa]	20 [MPa]	30 [MPa]

The diameter of the underground cavern is calculated with the relation (2) [31] (p. 58):

$$R = \sqrt{\frac{Q \cdot C_{sat}}{220 \cdot \pi \cdot w}}\ [\mathrm{m}] \quad (2)$$

where:

R – the radius of the dissolution cylinder;

Q – the flow of water introduced into the cavern, Q = 30 m^3/h;

C_{sat} – extracted brine concentration (saturated), in Kappeller degree (1 Kappeller degree = 10 grams / liter of brine), C_{sat} = 31.5 g/dm^3;

w – the lifting speed of the operating column, w = 0.00287 m/h, given by the relation (3) [31], (p. 59):

$$w = \frac{0.0167}{1000} \cdot {C_{sol}}^2\ [\mathrm{m/h}] \quad (3)$$

where: C_{sol} – solvent concentration in Kappeller degree = 13.1 g/dm^3;

For these parameters, resulted in a diameter of the underground reservoir of ~40 m. The dissolution massic speed of rock salt in the horizontal direction in [kg/(m^{2}h)] can be evaluated with the following empirical formula established by Külle (URSS) [32] (p. 59), [32] (p. 63), which also considers the salinity of the water introduced, in our case sea water:

$$V_{mass} = (3.25 \cdot \Psi^{0,5} + 1.8) \cdot \left(1 - \frac{C_{sol} \cdot \gamma_{sat}}{C_{sat} \cdot \gamma_{sol}}\right)\left(1 + \frac{t}{22.4}\right) = 5.82\ [\mathrm{kg/m^2 \cdot h}] \quad (4)$$

where: C_{sat} – the saturation concentration of the brine = 0.315 g/cm^3; C_{sol} – solvent concentration ~ 0.18 g/cm^3 (marine water in Vadu area, see above); Ψ – 1.57 rad (corresponds to the 90° angle made by the vertical wall of the dissolution chamber with the horizontal); γ_{sat} – the specific density of the saturated brine = 1.24 g/cm^3; γ_{sol} – the specific density of the solvent = 1.13 g/cm^3. To express the dissolving speed in [m/h] in radial direction, should be divided the V_{mass} obtained by Kulle's relation to the specific density of the salt γ_{salt} = 2160 kg/m^3 and in this case

$$V = \frac{V_{mass}\,(\text{from relation }(4))}{\gamma_{salt}} = 0.0027\ \mathrm{m/h} \quad (5)$$

The management of the dissolution is done through a rigorous control of the quantities of seawater introduced into the well, the quantities of brine extracted and its concentration, considering the initial salinity of the seawater. The completion time of a step can be calculated with the relation (6) [32]:

$$T = \frac{0.6 \cdot R}{V} = 203\ [\mathrm{days}] \quad (6)$$

where: R – radius of the underground reservoir, R = 20 m; V – mean radial velocity of dissolution = 0.0027 · 24 = 0.0648 m/day. Results the completion time of T = 200 days. For a radius of the

Preprints.org (www.preprints.org) | NOT PEER-REVIEWED | Posted: 17 February 2025 doi:10.20944/preprints202502.1207.v1

underground reservoir, R = 30 m, the completion time is T = 300 days. The optimal height of the dissolution step was determined by the relation (7) [15]:

$$h_{stage} = K_1 \cdot K_2 \cdot \frac{C_m \cdot Q}{\pi \cdot R \cdot V \cdot \gamma_{salt}} \text{ [m]} \quad (7)$$

where: K_1 – correction coefficient = 1.13; K_2 – coefficient that depends on the speed of salt dissolution = 14.4; γ_{salt} – the specific density of the salt (from above); V – mean radial velocity of dissolution = 0.065 m/day; C_m – medium concentration of brine = 166.5 g/dm^3.

In conclusion, for these parameters, the height of the dissolution step will be 8.7 m for a radius of the underground reservoir, R = 20 m, and 5.9 m for a radius of the underground reservoir, R = 30 m, in completion time of T = 200 days for the first case and T = 300 days for the second case. For the geomechanical conditions in the Vadu structure the parameters are: the thickness of the package of covering rocks and sea water, $h_1 = h_r + h_w$ = 700 m + 100 m = 800 m; volume density of the covering rocks, $\gamma = 2.0 \cdot 10^3$ kg/m^3; the diameter of the dissolution cylinder, D = 40 m; tensile strength of the salt, σ_{rt} = 1.4 N/mm^2; density of salt, g = 9.8 m/s^2 (standard gravity).

The thickness of the salt floor h_f see the relation below [15]:

$$h_f \geq \frac{n \cdot \gamma \cdot \cdot g \cdot D^2}{2 \cdot k_f \cdot k_s \cdot \sigma_{rt}} \cdot \left[1 \pm \sqrt{\frac{4 \cdot k_f \cdot k_s \cdot \sigma_{rt}}{n \cdot D^2 \cdot \gamma^2} q}\right]; \; h_f \geq 35 \text{ m} \quad \text{[m]} \quad (8)$$

where: D – the diameter of the reservoir; q – the load given by the covering rocks, sea water, and the contrapressure of the brine, k_f = 4.85 (the correction coefficient), k_s = 1.3 (safety coefficient) and n = 1. For q see Appendix A.

The calculation results are given in the tables below:

Table 4. Geometrical data of the investigation of caverns.

Parameter	Cavern A	Cavern B
Diameter [m]	40	60
Height [m]	120	120
Cavern total volume [m^3]	150,000	320,000
Cavern free volume [m^3]	100,000	225,000
Formation time/step	200 days/8.7 m=23 days/m	300 days/5.7 m=51 days/m
Total time for a cavern formation	2,760 days~92 month~8 years	6120 days~204 month~17 years
Depth to cavern ceiling from seabed [m]	700	1,400

The time is almost double as given in literature [15] due to the salinity of the see water used for cavern creation and that is lowering the proces.

In Table 6 below calculations are given over the hydrogen storage capacity of each type of cavern at the given depth of 700 m respectivelly 1,400 m. Also, the termal gradient with depths of about 30°/1,000m have been taken into consideration, see Table 5. Heve been taken into consideration the netto volume of hydrogen, the netto mass stored and the netto energy potential storage.

Table 5. Assumptions used in the cavern capacity calculations.

Parameter	Value
Seabed depth	20 ÷ 100 m
Fraction of total cavern volume used as cavern free volume	70%
Average temperature at wellhead	6°C

Preprints.org (www.preprints.org) | NOT PEER-REVIEWED | Posted: 17 February 2025 doi:10.20944/preprints202502.1207.v1

Maximum cavern pressure, measured at the LCCS (Last Cemented Casing Shoe)	$0.80 \cdot \sigma_v$
Minimum cavern pressure, measured at the LCCS	$0.20 \cdot \sigma_v$
Average temperature at seabed	9°C
Geothermal gradient	0.031°C/m

Table 6. Results of the calculations for the hydrogen storage capacity of the two investigated caverns.

Calculations results	Cavern A	Cavern B
Depth to cavern ceiling from seabed (m]	700	1,400
Geostatic vertical stress at the LCCS depth (bar)	150	290
Maximum cavern pressure, measured at the LCCS (bar-abs)	120	230
Minimum cavern pressure, measured at the LCCS (bar-abs)	30	60
Temperature at cavern mid-height (°C)	31	53
Cushion hydrogen required to maintain minimum cavern pressure (millions Nm^3)	2.75	11.16
Cushion hydrogen required to maintain minimum cavern pressure (tonnes)	245	996
Netto hydrogen volume (million Nm^3)	7.9	31.61
Netto hydrogen mass (tonnes)	704	2,821
Netto energy stored in the cavern (GWh)	23.443	93.939
Energy density per cavern (MWh/tonne)	33.3	

For a request of energy of 10 MWh at a given time, the energy stored in cavern A ensures a total functioning time of 2,344.3 hours ~ 97.7 days ~ 3 months and 1 week. Cavern B ensures a total functioning time of 9,393.9 hours ~ 391.4 days ~ 13 months (1 year and 1 month). Energy is a netto energy without taking into consideration the captived energy, that represents the minimum energy stored required for the correct functioning of such a storage system.

3. FEA Analysis of Underground Hydrogen Storage Caverns: Structural Integrity Under Pressure

To assess the structural integrity of underground hydrogen storage, finite element analysis (FEA) simulations were conducted on caverns located at two different depths: 700 m and 1400 m. The 3D models are at real scale. These caverns are subjected to varying hydrogen pressures, as shown in Table 6 above, the shallower cavern at 700 m operating within a range of 30–120 bar, while the deeper cavern at 1400 m experiences pressures between 60–230 bar.

The simulations aimed to evaluate the mechanical response of the surrounding salt deposit under these pressure conditions, identifying potential stress concentrations and failure points. The results provide insight into the feasibility of sustained hydrogen storage at different depths and pressure levels.

SolidWorks Simulation add-on was used to create and run the FEA analysis, due to its capability of defining custom materials. The caverns must withstand the lithostatic pressure exerted by the overlying rock strata and sea water. To account for this, an equivalent mass was determined based on the average density of each stratum and the mass of sea water above (shown in Figure 8. In order to be able to drill the 60 m caverns, they were interspersed between the 40 m ones. Also, in order to validate this result, the mass was also calculated based on geostatic pressure. Since SolidWorks does not support direct input of such high distributed mass values, an additional domain with an adjusted

Preprints.org (www.preprints.org) | NOT PEER-REVIEWED | Posted: 17 February 2025 doi:10.20944/preprints202502.1207.v1

density was introduced to replicate the correct weight. Series of simulations were done for both salt deposit and minimum and maximum cavern pressure. The matrix was simplified to 3x3 for 40 diameter caverns and 2x2 for 60 diameter caverns.

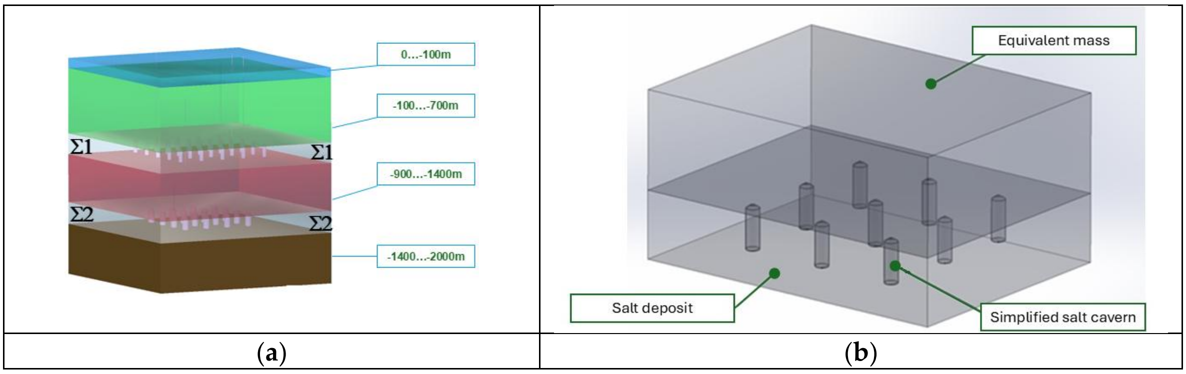

Figure 8. Simplification of domain of salt caverns. (**a**) individual 40m diameter cavern view; (**b**) top section view for 9 of 40 m diameter caverns.

In Figure 9 von Mises stress distribution across the first set of salt caverns is depicted (40m diameter, at 700m depth). The scale was limited to the lower value of compressive strength (22 MPa as of Table 2) showing that there is no risk of failure. It is shown that in the center of the matrix, the compressive strength is greater than at the margins.

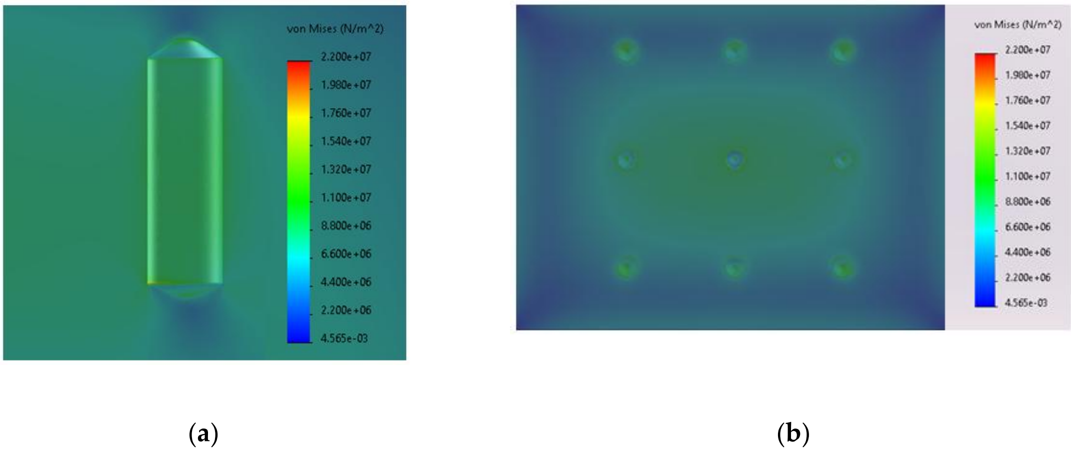

Figure 9. Mechanical stress of salt caverns at 120 bar internal pressure and 40m diameter; (**a**) individual cavern view; (**b**) top section view for 9 of 40 m diameter caverns.

In Figure 10 the scale was limited to the dilatation threshold (13 MPa as of Table 2), a point where the caverns will suffer plastic deformations.

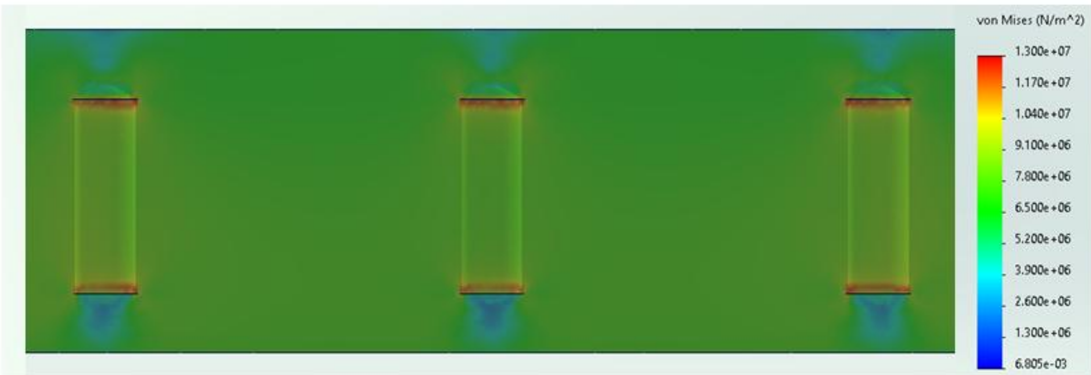

Figure 10. Tension at dilatation threshold for 120 bar internal pressure and 40m diameter.

For the minimum pressure of 30 bar, higher stress is seen at the extremities of the cylindrical part of the caverns, where the upper limit of the compressive strength is reached (36 MPa as of Table 2), which can be avoided by increasing the minimum pressure of the vessels, see Figures 11 and 12. The hidrogen withdrawal is available between 120 to 30 bar, and the cushion gas in conclusion should have 30 bar pressure minimum.

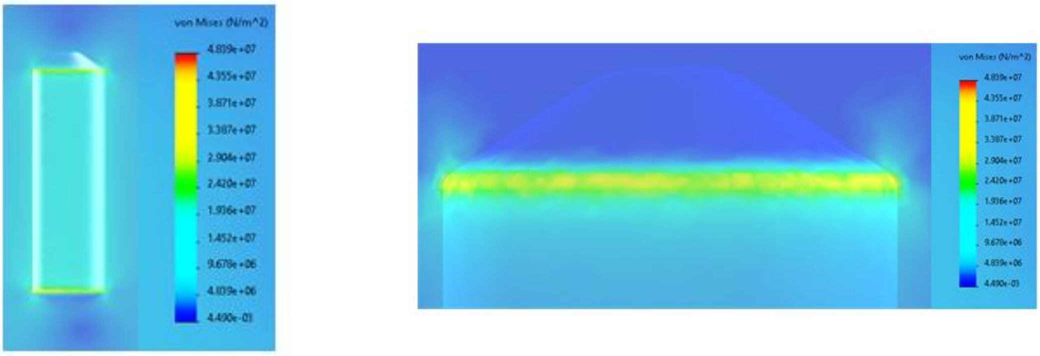

(**a**) (**b**)

Figure 11. Mechanical stress of salt caverns at 30 bar internal pressure and 40m diameter. (**a**) whole cavern view; (**b**) Detail at the top cavern view.

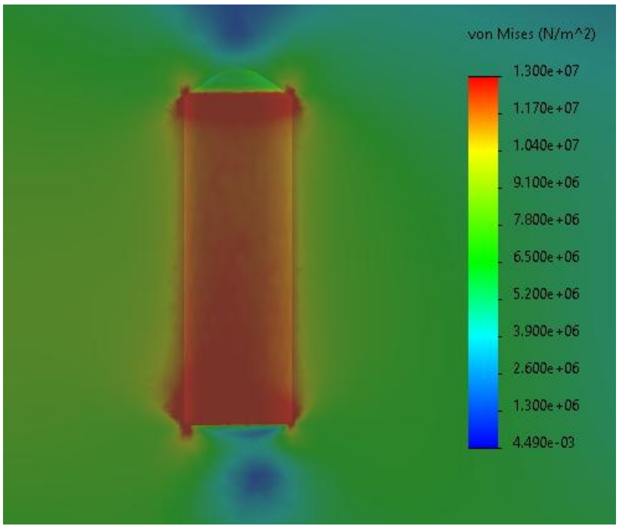

Figure 12. Tension at dilatation threshold for 30 bar internal pressure and 40m diameter.

At 1400m depth, since the geostatic pressure is much higher, this results in higher operating conditions of the caverns in order to avoid failure due to the exceeding of the compressive strength. At maximum operating pressure, at the extremities of the cylindrical part, some spots that are close to the compressive strength limit can be seen in Figures 13 and 14.

Preprints.org (www.preprints.org) | NOT PEER-REVIEWED | Posted: 17 February 2025 doi:10.20944/preprints202502.1207.v1

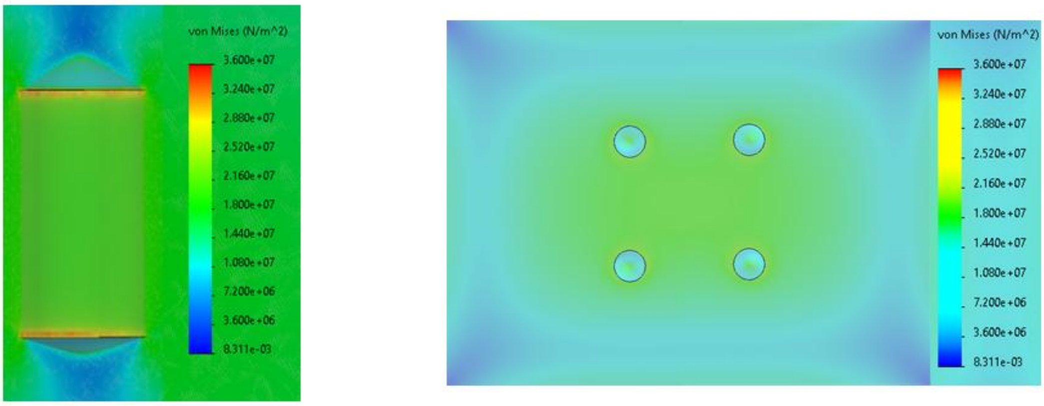

(**a**) (**b**)

Figure 13. Mechanical stress of salt caverns at maximum 230 bar internal pressure and 60m diameter. (**a**) individual cavern view; (**b**) top section view for 4 caverns.

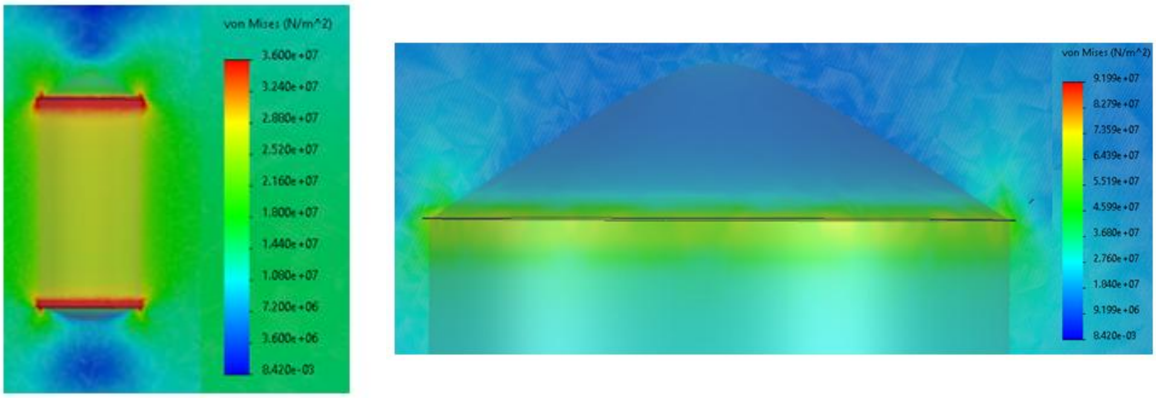

(**a**) (**b**)

Figure 14. Mechanical stress of salt caverns at minimum 60 bar internal pressure and 60m diameter. (**a**) whole cavern view; (**b**) Detail at the top cavern view, with rescaled tensions in the crical zone.

At the minimum pressure of 60 bar, a maximum stress of around 65 MPa is reached, that would result in a critical failure of the salt caverns, in the zone of the top and bottom cones. The conclusion is that it is not possible to withdraw the hidrogen under the pressure of 60 bar in the cavern at 1400 m depth. The hidrogen withdrawal is available between 230 to 60 bar, and the cushion gas in conclusion should have 60 bar pressure.

In Table 7 data have been collected for cavern storage sites indicated for drilling salt storage caverns [33].

Preprints.org (www.preprints.org) | NOT PEER-REVIEWED | Posted: 17 February 2025 doi:10.20944/preprints202502.1207.v1

Table 7. Key geological and industrial indicators for suitable sites.

Parameter	Criteria	Positive indicator score = 10	Intermediate indicator score = 5	Cautionary indicator score = 1	Reference
Host salt formation	Depth (m) (from seabed)	1000–1500	500–1000 and 1500–2000	<500 and >2000	Smith et al. (2005) [34]; Evans and Holloway (2009) [22]; Plaat (2009) [23]; Caglayan et al. (2020) [18]
	Thickness (m)	>400	200-400	<200	Caglayan et al. (2020) [18]; Allsop et al. (2023) [16];
	Purity (%)	>80	60-80	<60	Li et al. (2019) [35] ; Saltwork Consultants Pty Ltd (2021) [36];
	In situ stress state	Isotropic	Orthotropic	Anisotropic	Minkley et al. (2015) [37]; Li and Urai (2016) [38]; Zijp et al. (2018) [39] ; Urai et al. (2019) [40];
Load bearing rock formation (hanging and foot wall)	Lithology	Halite	Mudstone and K–Mg salts	Carbonate and anhydrite	Li et al. (2020) [41] ; Taheri et al. (2020) [42];
	Thickness (m)	Bedded hanging: >80; foot: >30	Bedded hanging: 63; foot: 16.8	Bedded hanging: <60; foot: <20	Bruno (2005) [43] ; Wang T. et al. (2015) [20]; Caglayan et al. (2020) [18];
		Diapiric hanging: >50; foot: >15	Diapiric hanging: >43.5; foot: 11.6	Diapiric hanging: <40; foot: <10	

	Structural features	None	Folding	Faults/fractures	Allsop et al. (2023) [16];
Lithological Interlayers If no interlayers, award score = 100	Lithology	K–Mg salts and polyhalite	Anhydrite and mudstone	Carbonates	Li and Urai (2016) [38]; Cala et al. (2018) [44]; Zijp et al. (2018) [39]; Urai et al. (2019) [40];
	Thickness (m) (non-salt)	<3 (single interlayer)	3 (single interlayer)	>3 (single interlayer)	Hamilton (1971) [45];
	Thickness (m) (K–Mg salts)	<3 (total thickness)	3–10 (total thickness)	>10 (total thickness)	Urai et al. (2019) [40];
	Location	Base	Centre	Top	Richter-Bernburg (1980) [46]; Li et al. (2019) [47];
	Number of interlayers	0	1 – 2	> 2	Li and Urai (2016) [38]; Cala et al. (2018) [44]; Zijp et al. (2018) [39]; Urai et al. (2019) [40];
Cavern geometry	Cavern volume (m^3)/ height (m)	750,000 (300)	500,000 (120)	n/a	Caglayan et al. (2020) [18];
	Distance from salt edge (m)	Bedded: 2000	Bedded: <2000, >500	> 500 m	Kupfer et al. (1998) [26]; Looff et al. (2003) [48];
		Diapiric: 1000	Diapiric: <1000, >500		Caglayan et al. (2020) [17];
Industrial	Pipeline infrastructure (km)	< 5	5 – 10	> 10	Allsop et al. (2023) [16];
	Distance from UK	< 50	50 – 80	> 80	Allsop et al. (2023) [16];

 doi:10.20944/preprints202502.1207.v1

coastline (km)	

4. Short Comparison Between H_2 Salt Cavern Storage and H_2 Hydrate Storage

The conventional H_2 storage options include salt caverns, saline aquifers, and depleted gas reservoirs. Generally, storing hydrogen in salt caverns is preferable as the cushion gas is very low comparativelly with the other solutions, and it can be implemented on a large scale once these caverns exist. If these do not exist, the salt caverns are created by solution mining in salt-rich formations and the costs with mining are about \$25.5/m^3 [49]. For a cavern of 150,000 m^3 at 700m depth, the cost of salt cavern creation is about \$3,825,000, without other costs that are about \$5,800,000 [49] taking into consideration the values from Table 6. As a first approximation, the cost of a new salt cavern at 700m depth is about \$10,000,000. For a cavern of 320,000 m^3 at 1400m depth, as a first approximation, the cost of a new salt cavern is about \$30,000,000 taking into consideration the values from Table 6, about 3 times greater than a cavern at 700 m depth, but the storage mass is about 4 times greater than the storage mass in the cavern located at 700m depth.

A new technology for hydrogen storage is hydrate-based H_2 storage, based on thermodynamic hydrate promoter. A pure H_2 hydrate can achieve 5.3 wt% H_2 storage capacity at extremely high pressures of 300 MPa at 249 K (-24°C). The addition of thermodynamic hydrate promoters (THPs), such as tetrahydrofuran (THF), 1,3-dioxolane (DIOX), cyclopentane (CP) in the 5.56 mol%, have shown promotion effect on shifting H_2 hydrate equilibrium to moderate pressure and temperature ranging from 8.3 MPa to 18.3 MPa and 277…284K (4…11°C) [50].

The technology of hydrate formation is promising as long as for 1000 kg of water (1 m^3 of water) there is 56 kg captured hydrogen, or 1.9MWh/ tone water captured energy in conformity with Table 6, taking into consideration the pure water. Also, for pure water hydrogen hydrate formation it is necessary to have a pressure of over 300 Mpa at low temperatures. Using 5.56 mol% thermodynamic hydrate promoters (THPs), the amount of hydrogen stored decreased at ~4.3wt% see Appendix B, but the pressures also decrease dramatically, with positive slightly above 0°C temperatures.

From [51] for an amount of stored H_2 = 5.4 milion Nm^3, the initial cost of implementing the hydrate technology is about 15.2 billion JPY or 99 milion USD. From the above the initial cost for implementing 2 caverns, one at 700m and the other one at 1400m, is about 40 milion USD, for an amount of 39.5 million Nm^3 H_2.

In conclusion from a rough estimation, hydrogen hydrate technology is a very promising one with a ratio of 1:6 costs compared to salt cavern storage technology up to date.

The advantage of salt cavern tehnology in offshore areas is that the technology does not require fresh water for dissolving and the technologies are quite well-known. The greatest desadvantage is that technology takes a very long time to create a new cavern.

The offshore hydrogen hubs are a necessity not just for Romania but also for other countries especially those with access to the sea and ocean for large capacity container ships transporting to reduce and eventually eliminate greenhouse gas (GHG) emissions from international shipping [52].

5. Conclusions

The storage of hydrogen in Romania, as it was said in the summary of the work, is included in the Romanian Energy Strategy 2016-2030 [53] regarding the development of production, transport and storage infrastructure in the development of reliable projects to reduce the carbon footprint, and not only, but especially in the creation of a clean and intelligent planet. There are laws implemented at the European level for the gradual reduction of the carbon footprint, such as the reduction of at least 40% in 2030 and 70% in 2050 compared to the levels recorded in 2008 of CO_2 emissions for transport units, especially naval which brings a huge contribution to marine and environmental pollution. Romania had in April 2024 about 3,000 MW (16.5%) represented by wind farms [54], and in March 2024 about 3,000 MW (16.5%) represented by photovoltaic farms (including the prosumers)

Preprints.org (www.preprints.org) | NOT PEER-REVIEWED | Posted: 17 February 2025 doi:10.20944/preprints202502.1207.v1

[55], which means 33% of the power installed in electricity production units in Romania. The energy given by regenerable sourses at maximum production is in summer. In the winter the production of the regenarable sourses decrease dramatically. The hydrogen storage strategy plays an important role in maintaining stability and uniformity of energy production.

For Romania, the implementing of the hydrogen storage in the Romanian Energy Strategy, is of capital importance in terms of the further development of hydrogen production and transport capacities, in the context in which renewable energy is rapidly developing and the need for decarbonization comes into force. There are also projects to introduce hydrogen into natural gas networks, as well as projects to introduce hydrogen into electrical and thermal energy production capacities like fuel plants, with new generation engines, see Siemens Energy Strategy [56]. The opening of storage capacities offshore to the Black Sea, also opens up the opportunity to use stored hydrogen in order to feed maritime and fluvial, commercial and military ships in order to mix conventional fuels with percentages of hydrogen to reduce de carbon footprint [57]. The total number of wells that could be opened in the area of the trapezoid shown in Figures 2 and 3 of about 595 km^2, taking into consideration the margins shown in table 1, considering a diapiric deposit, and both levels, is aproximativelly 20,600 (10,300 in the 700 m first level and 10,300 at the 1,400 m second level), considerring a diameter of 60 m for the cavern and a distance between them of 240m ($4 \cdot D$), see also the trapezoidal area from Figures 2 and 3, divided into 18+5.35 sectors of 441 wells each shown in Figure B1 from Appendix C.

The total capacity in tonnes is given (from table 6) by the relation:

$$\mathcal{N}_{mass\_stored} = 10{,}300 \cdot 704 + 10{,}300 \cdot 2{,}821 = 36{,}307{,}500\ tonnes\ H_2 \tag{9}$$

over 36 million tonnes H_2. The total amount of energy stored is given by relation (9):

$$\mathcal{E}_{total\_stored} = 10{,}300 \cdot 23.44 + 10{,}300 \cdot 93.939 \sim 1209 TWh\ (1.209 PWh) \tag{10}$$

over 1.2 PWh energy stored. The conclusion is that Romania is at the beginning of the road in terms of hydrogen storage capacities but has a huge potential in developing them and in increasing the production and transport capacities of hydrogen, ensuring a sustainable future in the Green Energy Sector.

Author Contributions: Conceptualization, S.P., S.D., I.V. and B.T.O; methodology, S.P., I.V, S.D; validation, B.T.O and S.P.; formal analysis, I.V., R.M.S. and M.T.S.; investigation, S.P. and S.M.R; resources, S.P., S.D., R.M.S., M.T.S., M.L.V. and I.V.; writing—original draft preparation, I.V. and M.T.S.; writing—review and editing, S.P.; visualization, M.L.V; supervision, S.M.R; project administration, S.M.R; funding acquisition, S.M.R.; software, M.T.S.; data curation, B.T.O and M.L.V. All authors have read and agreed to the published version of the manuscript.

Funding: This research received no external funding

Data Availability Statement: The authors confirm that the data supporting the findings of this study are available within the article [and/or] its supplementary materials.

Acknowledgments: In this section, you can acknowledge any support given which is not covered by the author's contribution or funding sections. This may include administrative and technical support, or donations in kind (e.g., materials used for experiments).

Conflicts of Interest: The authors declare no conflicts of interest.

Appendix A

Regardless of how the floor is considered, the load acting on it will be [15]:

$$q = q_0 + q_s - p \tag{A1}$$

Where q_0 is the weight of the salt floor, q_s represents the additional load exerted by the rocks located above the salt deposit and p represents the counterpressure exerted by the brine inside the void produced by dissolution. So, we have the relations below:

Preprints.org (www.preprints.org) | NOT PEER-REVIEWED | Posted: 17 February 2025 doi:10.20944/preprints202502.1207.v1

$$q_0 = \gamma_{salt} \cdot g \cdot h_f \quad \text{(A2)}$$

where h_f was defined in the work by relation (8)

$$q_s = \gamma_1 \cdot g \cdot h_r + \gamma_{sol} \cdot g \cdot h_w \quad \text{(A3)}$$

and

$$p = \gamma_{sat} \cdot g \cdot (h_f + h_r + h_w) \quad \text{(A4)}$$

where the specific density of the salt, $\gamma_{salt} = 2.16 \cdot 10^3$ kg/m^3; the specific density of the brine, $\gamma_{sat} = 1.24 \cdot 10^3$ kg/m^3; the specific density of the solvent water (see water), γ_{sol} –= 1.13 g/cm^3.

Appendix B

For pure hydrogen hydrate, 5.3 wt% (5.3 kg H_2 per 100 kg hydrate) corresponds to 53 kg of hydrogen per 1000 kg of hydrate. Adding 5.56 moles THPs will be slightly reduces the H_2 storage capacity, as part of the hydrate mass is replaced by the promoter. The molar mass for THP varies (e.g., for THF is about 72 g/mol, for DIOX is about 90 g/mol and for CP is about 70 g/mol). For a rough estimation, we can use the average molar mass of the THPs, about 72 g/mol [58]. 5.56mol% of THP implies 94.44mol% of water. The mass procent for water and THP are calculated by equations [59]:

$$Y_{H_2O} = \frac{X_{H_2O} M_{H_2O}}{X_{H_2O} M_{H_2O} + X_{THF} M_{THF}} \cdot 100 \quad \text{(B1)}$$

and

$$Y_{THP} = \frac{X_{H_2O} M_{H_2O}}{X_{H_2O} M_{H_2O} + X_{THP} M_{THP}} \cdot 100 \quad \text{(B2)}$$

where $X_{H_2O} = 94.44\%$; $M_{H_2O} = 18 g/mol$; $X_{THF} = 5.56\%$ and $M_{THP} = 72\ g/mol$

As results, Y_{H_2O} = 81% and Y_{THP} = 19% from 1000 kg hydrate.

The amount of H_2 will be

$$Q_{H_2} = Y_{H_2O} \cdot 53 = 43\ kg \quad \text{(B3)}$$

where Q_{H_2O} is the mass of H_2 storred in 1000 kg hydrate with5.56 mol% of THP.

Appendix C

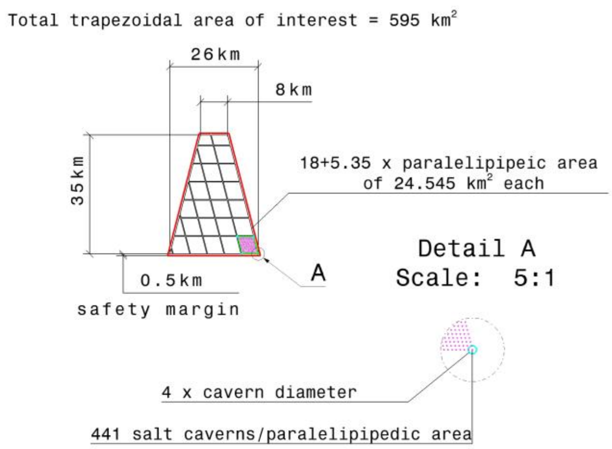

Figure A1. A schematic division of the trapezoidal sector from Figure 3, with the theoretical 10,300 wells per each level.

doi:10.20944/preprints202502.1207.v1

References

1. Hévin, G.; Underground storage of Hydrogen in salt caverns, European Workshop on Underground Energy Storage, Paris, France, 7th - 8th November 2019. Available online: https://energnet.eu/wp-content/uploads/2021/02/3-Hevin-Underground-Storage-H2-in-Salt.pdf (accesed on 29.10.2024)
2. Jahanbakhsh, A.; Potapov-Crighton, A. L.; Mosallanezhad A.; Tohidi Kaloorazi N.; Mercedes Maroto-Vale M.; Underground hydrogen storage: A UK perspective, *Renewable and Sustainable Energy Reviews*, **2024**, 189, Part B, 114001, https://doi.org/10.1016/j.rser.2023.114001
3. Zhu S.; Shi X.; Yang C.; Bai W.; Wei X.; Yang K.; Li P.; Li H.; Li Y.; Wang G.; Site selection evaluation for salt cavern hydrogen storage in China, *Renewable Energy*, **2024**, 224, 120143, https://doi.org/10.1016/j.renene.2024.120143
4. Parliament says shipping industry must contribute to climate neutrality. Press release. European Parliament, 16-09-2020. Available online: https://www.europarl.europa.eu/news/ro/press-room/20200910IPR86825/parliament-says-shipping-industry-must-contribute-to-climate-neutrality (accessed on 08.01.2025)
5. How much does the shipping industry contribute to global CO_2 emissions? GHG Emissions. Sinai SAS. September 22, 2023. Available online: https://sinay.ai/en/how-much-does-the-shipping-industry-contribute-to-global-co2-emissions/ (accessed on 08.01.2025)
6. Dimitriu R. G.; Oaie G.; Ranguelov B.; Radichev R.; Maps of the Gravity and Magnetic Anomalies for the Western Black Sea Continental Margin (Romanian - Bulgarian Sector), In Proceedings of 16th International Multidisciplinary Scientific GeoConference SGEM, 2016, **3**
7. Oaie G.; Florescu S.; Mare Nigrum – The First Romanian Multidisciplinary Research Vessel in Romania, In Proceedings of EuroEcoGeoCenter - Romania / Danube Delta, Romania, 2004, **No. 9-10.** Available online: https://geoecomar.ro/website/publicatii/Nr.9-10-2004/22.pdf (accesed on 29.10.2024)
8. Mare Nigrum. Ship of national interest. GeoEcoMar. Available online: https://geoecomar.ro/en/research-vessels/mare-nigrum/ (accessed on 08.01.2025)
9. Georgiev G.; Geology and Hydrocarbon Systems in the Western Black Sea, *Turkish Journal of Earth Sciences*, 2012, **21**, (5), 4, https://doi.org/10.3906/yer-1102-4
10. Flores M. N.; Aleman C. O.; Orozco-del-Castillo M. G.; Fucugauchi J. U.; Castellanos A. R.; Castañeda C. C.; Alcantara A. T.; 3D Gravity Modeling of Complex Salt Features in the Southern Gulf of Mexico, *International Journal of Geophysics*, 2016, Article ID 1702164, http://dx.doi.org/10.1155/2016/1702164
11. Prutkin I.; Saleh A.; Gravity and magnetic data inversion for 3D topography of the Moho discontinuity in the northern Red Sea area, Egypt, *Journal of Geodynamics*, 2009, **47**, 5, pp. 237-245, https://doi.org/10.1016/j.jog.2008.12.001
12. Prutkin I.; Vajda P.; Jahr T.; Bleibinhaus F.; Novák P.; Tenzer R., Interpretation of gravity and magnetic data with geological constraints for 3D structure of the Thuringian Basin, Germany, *Journal of Applied Geophysics*, 2017, **136**, pp. 35–41, http://dx.doi.org/10.1016/j.jappgeo.2016.10.039
13. Juravle D. T., In *Geologia Romaniei, Vol. 1, Geologia terenurilor Est-Carpatice (Platformele şi Orogenul Nord-Dobrogean) (Romanian Geology, Vol. 1, Geology of the Eastern Carpathian lands (Platforms and the North Dobrogean Orogen))*, Editura STEF, Iasi, Romania, 2009, ISBN: 978-973-1809-55-7, 2009. Available online: https://doru.juravle.com/publicatii/geologia_romaniei_vol01.html (accesed on 29.10.2024)
14. Dinu C.; Wong H. K.; Tambrea D.; Matenco L., Stratigraphic and structural characteristics of the Romanian Black Sea shelf, *Tectonophysics* 2005, **410**, (1) pp. 417–435, http://dx.doi.org/10.1016/j.tecto.2005.04.012
15. Coteş D., Studiul geomecanic al masivului de sare din structura Vadu în vederea executării unui rezervor de gaze naturale (Geo-mechanical study of Vadu salt deposit, in view of the construction of an underground natural gas storage facility), PhD. Thesis, University of Petroşani, Faculty of Mines, Petroşani, Romania, 2008
16. Hui S., Yin S., Pang X., Chen Z., Shi K., Potential of Salt Caverns for Hydrogen Storage in Southern Ontario, Canada, Mining 2023, 3, pp. 399–408, https://doi.org/10.3390/mining3030024
17. Popescu S., Radu M. S., Vîlceanu F., Dinescu S., Research on the setting of maximum pressure in salt caverns intended for CO_2 storage, MATEC Web of Conferences, 2022, **373**, 00066, https://doi.org/10.1051/matecconf/202237300066

18. Caglayan D. G.; Weber N.; Heinrichs H. U.; Linßen J.; Robinius M.; Kukla P. A.; Stolten D., Technical potential of salt caverns for hydrogen storage in Europe, *International Journal of Hydrogen Energy*, 2020, **45**, pp. 6793–6805, https://doi.org/10.1016/j.ijhydene. 2019.12.161
19. Wang L.; Bérest P.; Brouard B., Mechanical behavior of salt caverns: closed-form solutions vs numerical computations, *Rock Mechanics and Rock Engineering*, 2015, **48**, pp. 2369–2382, https://doi.org/10.1007/s00603-014-0699-1
20. Wang T.; Yang C.; Ma H.; Daemen J. J. K.; Wu H., Safety evaluation of gas storage caverns located close to a tectonic fault, *Journal of Natural Gas Science and Engineering*, 2015, **23**, pp. 281–293, https://doi.org/10.1016/j.jngse.2015.02.005
21. Lux K. H., Design of salt caverns for the storage of natural gas, crude oil and compressed air: geomechanical aspects of construction, operation and abandonment, *Geological Society*, Special Publications, London, 2009, **313**, pp. 93–128, https://doi.org/10.1144/SP313.7
22. Evans D. J.; Holloway S., A review of onshore UK salt deposits and their potential for underground gas storage. *Geological Society*, Special Publications, London, 2009, **313**, pp. 39–80, https://doi.org/10.1144/SP313.5
23. Plaat H., Underground gas storage: why and how, *Geological Society*, Special Publications, London, 2009, **313**, pp. 25–37, https://doi.org/10.1144/SP313.4
24. Ozarslan A., Large-scale hydrogen energy storage in salt caverns, *International Journal of Hydrogen Energy*, 2012, **37**, pp. 14265–14277, https://doi.org/10.1016/j.ijhydene.2012.07.111
25. Stolzenburg, K.; Hamelmann, R.; Wietschel, M.; Genoese, F.; Michaelis, J.; Lehmann, J.; Miege, A.; Krause, S.; Donadei, S.; Crotogino, F.; Acht, A.; Sponholz, C. & Horvath, P.-L. (2014). Integration von Wind-Wasserstoff-Systemen in das Energiesystem. Abschlussbericht. Planungsgruppe Energie und Technik (PLANET); Fachhochschule Lübeck (FH Lübeck); Fraunhofer Institut für System- und Innovationstechnik (ISI); Fachhochschule Stralsund (FH Stralsund); Underground Technologies (KBB). Available online: https://www.planet-energie.de/de/media/Abschlussbericht_Integration_von_Wind_Wasserstoff_Systemen_in_das_Energiesystem.pdf (accesed on 29.10.2024)
26. Kupfer D. H.; Lock B. E.; Schank P. R., Anomalous zones within the salt at Weeks Island, Louisiana, *Gulf Coast Association of Geological Societies Transactions*, 1998, **48**, pp. 181–192
27. Exploatarea zacamintelor de sare din Romania (II), (Exploitation of salt deposits in Romania (II)), Univers Ingineresc nr. 4/2015. Available online: https://www.agir.ro/univers-ingineresc/numar-4-2015/exploatarea-zacamintelor-de-sare-din-romania-ii_4763.html (accesed on 29.10.2024)
28. Stoica C.; Gherasie I., *Sarea şi sărurile de potasiu şi magneziu din România (Halite and potassium and magnesium salts from Romania)*, Editura tehnică, 1981, Bucureşti, Romania
29. Raport privind starea mediului marin şi costier în anul 2022 (Report on the state of the marine and coastal environment in 2022), Institutul National de Cercetare-Dezvoltare Marina „Grigore Antipa" (National Institute for Marine Research and Development "Grigore Antipa"). Available online: https://www.anpm.ro/documents/18093/81141723/2022+Capitolul+II.3+Mediul+marin+si+costier.pdf/08610e93-db2a-4c05-887e-e0980b2f7b35 (accesed on 29.10.2024)
30. Furst S. L.; Doucet S.; Vernant P.; Champollion C.; Carme J. L.; Monitoring surface deformation of deep salt mining in Vauvert (France), combining InSAR and leveling data for multi-source inversion, *Solid Earth*, 2021, **12**, pp. 15–34, https://doi.org/10.5194/se-12-15-2021
31. Popescu P., *Analiza stabilității golurilor și riscurile miniere din exploatările de sare în soluție din românia, în vederea utilizării acestora ca depozite subterane (Analysis of void stability and mining risks in solution salt mines in Romania, with a view to their use as underground storage)*, PhD. Thesis, University of Petroşani, Faculty of Mines, Petroşani, Romania, 2023
32. Paul C., *Exploatarea sării prin sonde (Exploitation of salt through wells)*, Editura Asociaţiei "S.I.P.G.", 2006, Bucureşti, Romania
33. Allsop C.; Yfantis G.; Passaris E.; Edlmann K., Utilizing publicly available datasets for identifying offshore salt strata and developing salt caverns for hydrogen storage, Geological Society, London, Special Publications, 2023, 528, pp. 139 – 169, https://doi.org/10.1144/sp528-2022-82

Preprints.org (www.preprints.org) | NOT PEER-REVIEWED | Posted: 17 February 2025 doi:10.20944/preprints202502.1207.v1

34. Smith N. J. P.; Evans D. J.; Andrew I., The geology of gas storage in offshore salt caverns. Marine, Coastal and Hydrocarbons Programme, British Geological Survey, 1–22. Confidential Report to the Department of Trade and Industry No. GC05/11, 2005
35. Li J.; Tang Y.; Shi X.; Xu W.; Yang C., Modeling the construction of energy storage salt caverns in bedded salt. *Applied Energy*, 2019, **255**, 113866, https://doi.org/10.1016/j.apenergy.2019.113866
36. Solution Mining, Saltwork Consultants Pty Ltd. Available online: https://www.saltworkconsultants.com/solution-mining/ (accessed on 08.01.2025)
37. Minkley W.; Knauth M.; Fabig T.; Farag N., Stability and integrity of salt caverns under consideration of hydro-mechanical loading, *IfG Institut für Gebirgsmechanik GmbH*, 2016. Available online: https://www.researchgate.net/publication/283871641_Stability_and_integrity_of_salt_caverns_under_consideration_of_hydro-mechanical_loading (accessed on 29.10.2024)
38. Li S.; Urai J., Numerical modelling of gravitational sinking of anhydrite stringers in salt (at rest). *Bollettino di Geofisica Teorica e Applicata*, 2016, **57**, pp. 233–246, https://doi.org/10.4430/bgta0178
39. Zijp M. H. A. A.; Huijgen M. A.; Wilpshaar M.; Bouroullec R. J.; ter Heege H., Stringers in Salt as a Drilling Risk. Report no. TNO2018 R10975 by Nederlandse Organisatie voor Toegepast Natuurwetenschappelijk Onderzoek for Dutch State Supervision of Mines, 2018
40. Urai J. L.; Schmatz J.; Kalver J., Over-pressured Salt Solution Mining Caverns and Leakage Mechanisms. Report, Project KEM-17, Phase 1: Micro-scale processes, 2019. Available online: https://kemprogramma.nl/file/download/a22c0dda-017d-4ecf-9f72-a911d9c51b5c/kem-17-kem-deepnl-colloquium-overpressured-caverns-presentatie-sodm-7-oktober-2021.pdf (accessed on 29.10.2024)
41. Li W.; Miao X.; Yang C., Failure analysis for gas storage salt cavern by thermo-mechanical modelling considering rock salt creep, *Journal of Energy Storage*, 2020, **32**, 102004, https://doi.org/10.1016/j.est.2020.102004
42. Taheri S. R.; Pak A.; Shad S.; Mehrgini B.; Razifar M., Investigation of rock salt layer creep and its effects on casing collapse, *International Journal of Mining Science and Technology*, 2020, **30**, pp. 357–365, https://doi.org/10.1016/j.ijmst.2020.02.001
43. Bruno M. S., Geomechanical Analysis and Design Considerations for Thin-bedded Salt Caverns. Final report no. DE-FC26-03NT41813, GTI Contract 8701. Terralog Technologies Inc., Arcadia, CA, 2005
44. Cala M.; Cyran K.; Kowalski M.; Wilkosz P., Influence of the anhydrite interbeds on a stability of the storage caverns in the Mechelinki salt deposit (Northern Poland). *Archives of Mining Sciences*, 2018, **63**, pp. 1007–1025, https://doi.org/10.24425/ams.2018.124990
45. Hamilton W. N., Salt in east-central Alberta. Research Council of Alberta, *RCA/AGS Bulletin*, 1971, **29**, 65
46. Richter-Bernburg G., Salt tectonics, interior structures of salt bodies. *Bulletin des Centres de Recherches Exploration-Production Elf-Aquitaine*, 1980, **4**, pp. 373–393,
47. Li J.; Tang Y.; Shi X.; Xu W.; Yang C., Modeling the construction of energy storage salt caverns in bedded salt, *Applied Energy*, 2019, **255**, 113866, https://doi.org/10.1016/j.apenergy.2019.113866
48. Looff K.; Duffield J.; Looff K., Edge of salt definition for salt domes and other deformed salt structures – geologic and geophysical considerations, *Solution Mining Research Institute Technical Conference*, 2003, Houston, TX, United States of America
49. F. Chen, Z. Ma, H. Nasrabadi, B. Chen, M. Z. Saad Mehana, J. Van Wijk, Capacity assessment and cost analysis of geologic storage of hydrogen: A case study in Intermountain-West Region USA, IJHE **48** (2023) 9008-9022, https://doi.org/10.1016/j.ijhydene.2022.11.292
50. J. Zhang, Yan Li, Y. Rao, Yang Li, T. He, P. Linga, X. Wang, Q. Chen, Z. Yin, Probing the pathway of H2-THF and H2-DIOX sII hydrates formation: Implication on hydrate-based H2 storage, Applied Energy **376** (2024) 124289, https://doi.org/10.1016/j.apenergy.2024.124289
51. T. Shibata, H. Yamachi, R. Ohmura, Y. H. Mori, Engineering investigation of hydrogen storage in the form of a clathrate hydrate: Conceptual designs of underground hydrate-storage silos, IJHE, **37**, 9, 2012, pp. 7612-7623, https://doi.org/10.1016/j.ijhydene.2012.02.037
52. D. Rutherford, X. Mao, B. Comer, Potential CO_2 reductions under the Energy Efficiency Existing Ship Index, ICCT WORKING PAPER 2020-27, 2020. Available online:

https://www.researchgate.net/publication/345950880_Potential_CO_2_reductions_under_the_Energy_Efficiency_Existing_Ship_Index. (accessed on 13.02.2025)

53. Romanian Energy Strategy 2016-2030, With an Outlook to 2050. Executive Summary, Ministry of Energy. Available online: https://energie.gov.ro/wp-content/uploads/2016/11/Romanian-Energy-Strategy-2016-2030-executive-summary3-1.pdf (accessed on 29.10.2024)
54. Dogar A., Producători de energie eoliană în România. Lista completă a centralelor în 2024 (Wind energy producers in Romania. Complete list of power plants in 2024), GreatNews, April 4, 2024. Available online: https://onoff.greatnews.ro/producatori-de-energie-eoliana-in-romania-lista-completa-a-centralelor-in-2024/ (accessed on 08.01.2025)
55. Nicut M., Premieră: România a depășit pragul de 1.000 MW producție instantanee de energie solară pentru prima dată în istorie (Premiere: Romania has exceeded the threshold of 1,000 MW of instantaneous solar energy production for the first time in history), ECONOMICA.net, March 4, 2024. Available online: https://www.economica.net/premiera-romania-a-depasit-pragul-de-1-000-mw-productie-instantanee-de-energie-solara-pentru-prima-data-in-istorie_729357.html (accessed on 08.01.2025)
56. EWE, Siemens Energy to build 280 MW green hydrogen electrolysis plant, Reuters, July 25, 2024. Available online: https://www.reuters.com/sustainability/climate-energy/ewe-siemens-energy-build-280-mw-green-hydrogen-electrolysis-plant-2024-07-25/ (accessed on 08.01.2025)
57. Vlăducă I.; Nechifor C. V.; Vasile M. L.; Suciu C. P.; Badea P. G.; Stănescu T.; Nicoară R. E.; Prisăcariu E. G.; Stanciuc R. M.; Popescu S.; Dinescu S.; Obreja A. M., Hydrogen Storage in Offshore Salt Caverns for Reducing Ships Carbon Dioxide Footprint, *Technium: Romanian Journal of Applied Sciences and Technology* (ISSN: 2668-778X), 2022, **4**, 9, https://doi.org/10.47577/technium.v4i9.7547
58. Tetrahydrofuran. National Library of Medicine. Available online: https://pubchem.ncbi.nlm.nih.gov/compound/Tetrahydrofuran. (accessed on 13.02.2025)
59. P.A. O'Neill, Industrial compressors. Theory and equipment. Butterworth-Heinemann Ltd, Linacre House, Oxford, Great Britain, 1993. ISBN 0-7506-0870-6